ZnO/Perovskite core-shell nanorod array based monolithic catalysts with enhanced propane oxidation and material utilization efficiency at low temperature

Sibo Wang, ¹ Zheng Ren, ¹ Wenqiao Song, ² Yanbing Guo, ^{1,*} Mingwan Zhang, ¹ Steven L. Suib, ^{1, 2} Pu-Xian Gao*, ¹

University of Connecticut, Storrs, CT 06269-3136, USA

Corresponding authors: puxian.gao@ims.uconn.edu, yanbing.guo@ims.uconn.edu,

KEYWORDS: metal oxide, core-shell nanorod arrays, monolithic catalyst,

heterogeneous catalysis, low temperature propane oxidation

Abstract

A hydrothermal strategy combined with colloidal deposition synthesis was successfully used to grow ZnO/perovskite (LaBO₃, B=Mn, Co, Ni) core-shell nanorod arrays within three dimensional (3-D) honeycomb cordierite substrates. A facile sonication assisted colloidal wash coating process is able to coat a uniformly dispersed perovskite nanoparticles onto the large scale ZnO nanorod arrays rooted on the channel surfaces of the 3D cordierite substrate achieved by hydrothermal synthesis. Compared to traditional wash-coated perovskite catalysts, an enhanced catalytic performance was observed for propane oxidation with 25°C lower light-off temperature than wash-coated perovskite catalyst of similar LaMnO₃ loading (4.3mg). Temperature programmed reduction and desorption under H₂ and O₂ atmosphere, respectively, were used to study the reducibility and oxygen activity of these core-shell nanorod arrays based monolithic catalysts, revealing a catalytic activity sequence of LaCoO₃>LaMnO₃>La₂NiO₄ at the initial stage of catalytic reaction. The good dispersion and size control in La-based perovskite nanoparticles and their interfaces to ZnO nanorod arrays support may contribute to the enhancement of catalytic performance. This work may provide a new type of Pt-group metals (PGM) free catalysts with improved catalytic performance for hydrocarbon oxidations at low temperatures.

¹Department of Materials Science and Engineering & Institute of Materials Science,

²Department of Chemistry, University of Connecticut, Storrs, CT 06269, USA

Introduction

The rapid consumption of platinum-group metals (PGM) and increasingly stringent exhaust emission restrictions impose a critical challenge for scientists and engineers to achieve sustainable energy and environment globally [1,2]. While pursuing energy efficiency and critical materials saving, as well as environmental pollution control, the environmental friendly and fuel-efficient low temperature combustion (LTC) technology represents a promising approach to be adopted as an upcoming solution. This, however, is in need of a compatible catalytic aftertreatment technology that can address the lack of low temperature catalytic activity in commercially available catalysts during cold start of automotive engines. Perovskite type materials, especially lanthanum based metal oxides have been widely investigated in the past decade as promising catalysts for hydrocarbon oxidation that possesses good stability at elevated temperature but suffer from compromised activity and high light-off temperature [3-6]. Solutions have yet to be found for the inevitable trade-off between poor catalytic activity at low temperature and thermal stability at high temperature [7]. Moreover, traditional particle-form perovskite based monolith catalysts heavily rely on empirical wash-coating processes with general morphology lacking of well-defined structure [8]. Recently, nanostructure array based monolithic catalysts have been proposed, which may provide a promising solution to bridge the gap between catalytic performance and utilization efficiency of materials [8,9]. Furthermore, we have successfully demonstrated the scalable integration of cordierite honeycomb with $M_XCo_{3-X}O_4$ (M = Co, Ni, Zn) nano-array catalysts using a cost-effective low temperature hydrothermal method, offering great enhancement in terms of methane oxidation performance and material usage efficiency [9].

Herein, we report a cost effective two-step (hydrothermal and colloidal deposition) sequential synthesis approach to integrate commercial 3-D monolithic cordierite honeycomb with uniformly distributed ZnO/LaBO₃ (B = Co, Mn, Ni) core-shell nanorod arrays. Compared to traditional LaMnO₃ powder wash-coated monolithic catalysts, the ZnO/LaMnO₃ nano-array based structured catalyst shows significant enhancement of catalytic propane oxidation performance by lowering the activation energy and reducing the light-off temperature more than 25°C. A series of characterization techniques were used to investigate the reducibility and oxygen activity of different types of ZnO/perovskite core-shell nanorod arrays based monolithic catalysts.

Experimental methods:

To synthesize the core-shell nanorod arrays based monolithic catalysts, a two-step process was used. First, ZnO nanorod arrays were grown upon 3D multi-channeled cordierite substrate using hydrothermal method. And then perovskite-type metal oxide film was conformably deposited onto ZnO nanorod arrays on honeycomb monoliths. Before ZnO nanostructure growth, a seeding layer of ZnO was deposited on $10 \times 10 \text{ mm}^2$

bare cordierite substrates through a sonication-assisted dip coating method [10]. The ZnO nanostructures were achieved using a 200ml aqueous solution with equal molar amount of zinc acetate and hexamine (HMT) (12.5mM). The seeded substrate was submerged under mixed solution with magnetically stirring at 500rpm and heated at 80°C. The aqueous solution was refreshed every 6 hours and after three cycles of growth, the substrate was rinsed with ethanol and dried naturally. In the second step, firstly, three types of LaBO₃ (B = Mn, Co, Ni) colloidal solution were prepared by dissolving the stoichiometric metal nitrates (0.12 M) in 20 ml ethoxyethanol under sonication. Once the precursors were completely dissolved, 0.11g polyvinylpyrrolidone (PVP Mw 58000) and 0.15 ml diethanolamine were added under vigorous stirring, after which the solutions became cloudy and followed by 72 hours ageing. The perovskite film was deposited on ZnO nanorod arrays using a simple wash coating method. The ZnO nanorod arrays integrated substrate was submerged under the colloidal solution and sonicated for 1 minute. Then the substrate was transferred to a furnace and dried at 300°C for 10 minutes. The wash-coating process was repeated for 8 times and followed by annealing at 650°C for 1 hour with a ramping rate 5°C/min to enhance crystallinity of metal oxides. In 10 batches of the repeated wash-coating processes, the weight loading ratio of perovskites (e.g. LMO) is in a range of 5.8% - 6.0%, showing good reproducibility of the sonication assisted colloidal deposition in terms of perovskite loading amount.

The X-ray diffraction pattern on the prepared nano-array structures was acquired using a BRUKER D2 X-ray diffractometer (Cu K α radiation, λ =1.540598Å). The morphology and structure of nano-array catalysts were characterized using a field emission scanning electron microscope (FE-SEM, JEOL 6335F) and a high resolution transmission electron microscope (HRTEM, JEOL JEM-2010, 200 KV). The BET surface areas of catalysts were determined by a Micromeritics ASAP 2020 Automatic Chemisorption Analyzer.

The catalytic performance of propane oxidation over nanorod array monolithic catalysts was carried out using a home-built bench reactor. The inlet was attached to gas delivery system controlled by a gas mixing box, and the outlet connected to a Fourier transform infrared spectrometer (FTIR, Thermo-fisher Nicolet 6700) to analyze the composition and concentration of effluent gas. Four pieces of 2mm × 2mm × 1cm ZnO/LaBO₃ nanoarray integrated cordierite honeycombs were aligned in a row in a stainless steel tube for propane oxidation evaluation. Quartz wool was placed at both ends to keep the samples' position fixed under gas flow. Before the catalytic test, the samples were treated in pure nitrogen (500ml/min) flow for 30 minutes at 150°C to eliminate residual air and water phase in the stainless steel tubes. During the catalytic test, the inlet gas was composed of 1% propane and 8% oxygen balanced with nitrogen with a flow rate of 150ml/min and a space velocity of 56250 h⁻¹.

The temperature programmed reduction of H₂ (H₂-TPR) and desorption of O₂ (O₂-TPD) mass spectrometry analysis were conducted in a tube furnace equipped with a gas

analyzer MKS coupled with a quadruple mass selective detector whose temperature was controlled by the WATLOW F4 controller. In both experiments, 1.0g as-prepared monolithic sample was ground into coarse powders and filled into a quartz tube. The sample was first purged under a flow of argon at 300°C for 1 hour, then cooled down to room temperature. After purging, the catalyst was heated under a mixed gas flow of hydrogen and argon (H₂: Ar = 1 : 4) from room temperature to 800°C with a ramping rate of 10°C/min. For O₂-TPD, the catalyst was exposed in pure oxygen for 1 hour and purged with argon for 30min at room temperature. Then the catalyst was heated up to 1000°C in a flow of argon. The flow rate in every step was maintained at 200 sccm.

Results and discussion:

Table 1 lists physical characteristics of ZnO nanorod arrays, LMO powder, and core-shell nanorod arrays based cordierite samples. After 8 times of wash-coating, the perovskite materials loading ratio can be controlled at around 12 g/L. The BET surface areas of these samples are also presented in the table. The BET surface areas of nano-array rooted on cordierite substrate surfaces were calculated based on Equation 1.

$$S_A = \frac{S_M * W_M - S_{BC} * W_{BC}}{W_A}$$
 Equation 1

The BET surface areas of perovskite film coated on ZnO nanorod array were calculated according to the following Equation 2.

$$S_P = \frac{S_M * W_M - S_{ZM} * W_{ZM}}{W_P}$$
 Equation 2

 S_A and W_A : Surface area and weight of nano-array on cordierite

 S_P and W_P : Surface area and weight of perovskite nanoparticles.

 S_{BC} and W_{BC} : Surface area and weight of bare cordierite

 S_M and W_M : Surface area and weight of monolithic samples

 S_{ZM} and W_{ZM} : Surface area and weight of ZnO/cordierite monolithic sample

For LMO/cordierite sample, the BET surface area of LMO was calculated in a similar way based on the tested BET results of bare cordierites.

Table 1.

Physical property	BET of monolithic sample m²/g	Perovskite concentration based on ICP- AES result (mg/g)	Perovskite weight/volume loading ratio (g/L)	Calculated BET of nano-arrays (m²/g)	Calculated BET of perovskite (m²/g)	Catalysts for propane oxidation test (mg)	Perovskite material usage for test (mg)
Bare cordierite	0.36						
ZnO/cordierite	1.43			15.6		93.0	None
LMO/cordierite	1.55	49.7	12.2		24.3	89.0	4.42
ZnO/LMO cordierite	1.73	41.8	10.2	12.6	8.6	98.2	4.10
ZnO/LCO cordierite	1.62	51.5	12.6	10.4	5.12	94.4	4.86
ZnO/LNO cordierite	2.10	44.7	10.9	15.2	16.4	96.3	4.30

X-ray diffraction analysis was conducted on the ZnO/perovskite nano-array monolithic catalysts. As a reference, the XRD pattern was collected on the perovskite powders synthesized from identical colloidal solution prepared for the nano-array based catalysts. LaMnO_{3.5} (PDF 32-0484), LaCoO₃ (PDF 25-1060), La₂NiO₄ (PDF 89-3460), ZnO (PDF 36-1451) and cordierite (PDF 12-0303) were detected.

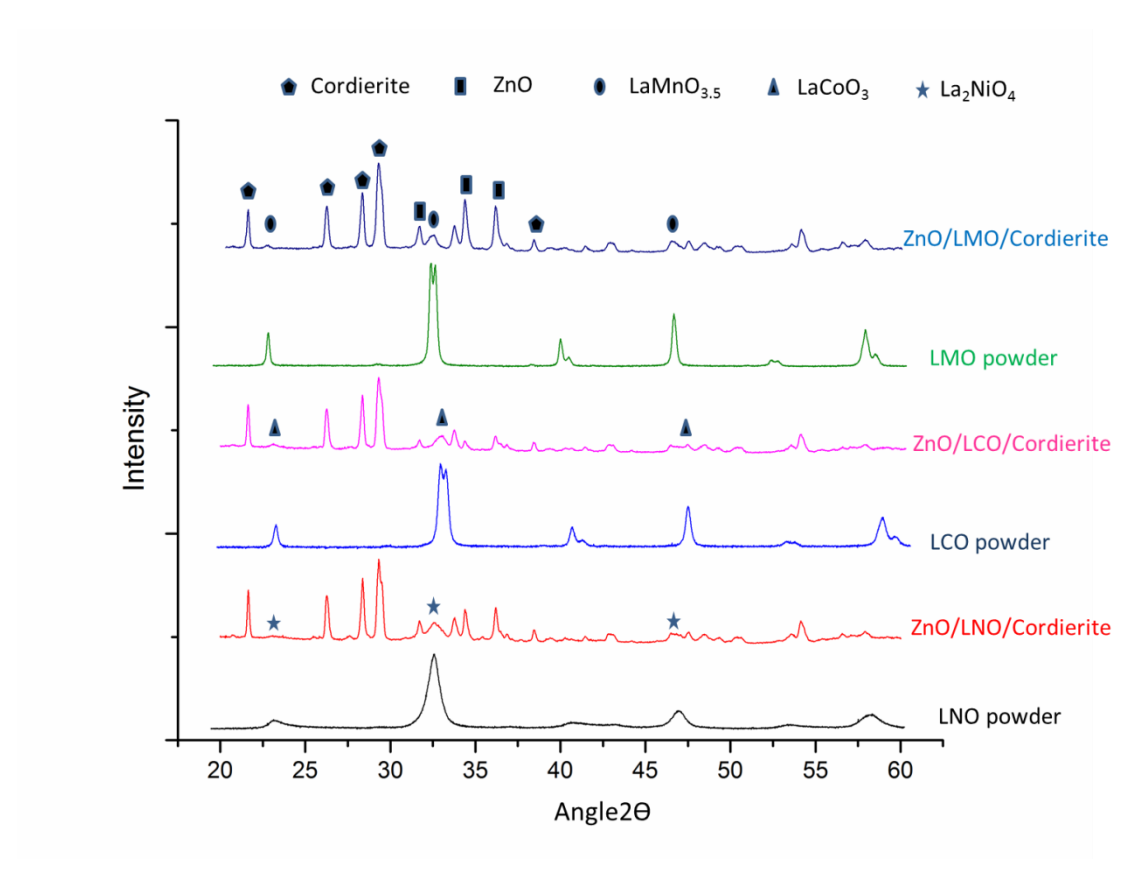


Figure 1. X-ray diffraction patterns of nanorod arrays based catalysts and perovskite powders

Figures 2 (a) and (b) present typical morphology of ZnO nanorod arrays that uniformly rooted on the monolithic substrate channel surface. The weight loading ratio of ZnO

nanorods is around 7% after 3 cycles of hydrothermal growth. The nanorod array displays a length of ~1.5 µm and a diameter of 150 nm- 200 nm. The geometry of ZnO nanorods could be tuned by the growth parameters such as temperature and precursor solution concentration [10]. Figure 2 (d), (e) and (f) display the top view and Figure 2 (g), (h) and (k) show the cross-sectional view of the three types of ZnO/perovskite core-shell nanorod arrays. Energy dispersive X-ray spectroscopy (EDS) confirmed the successful loading of perovskite nano-shell. Taking ZnO/LMO Figure 2 (c) as an example, the atomic ratios of Zn, Mn, La elements are 83.6%, 8.0%, and 8.4%, respectively. The vertically aligned structural characteristic was well retained after perovskite film loading on ZnO nanorod arrays. The profiles of perovskite films on ZnO nano-arrays can be clearly observed in the respective cross-section SEM images Figure 2 (g)-(k). Among the three types of coreshell nano-arrays, ZnO/LaCoO₃ nanorods possess a relatively rougher surface, indicating distribution LaCoO₃ nanoparticle larger size of wash-coated film.

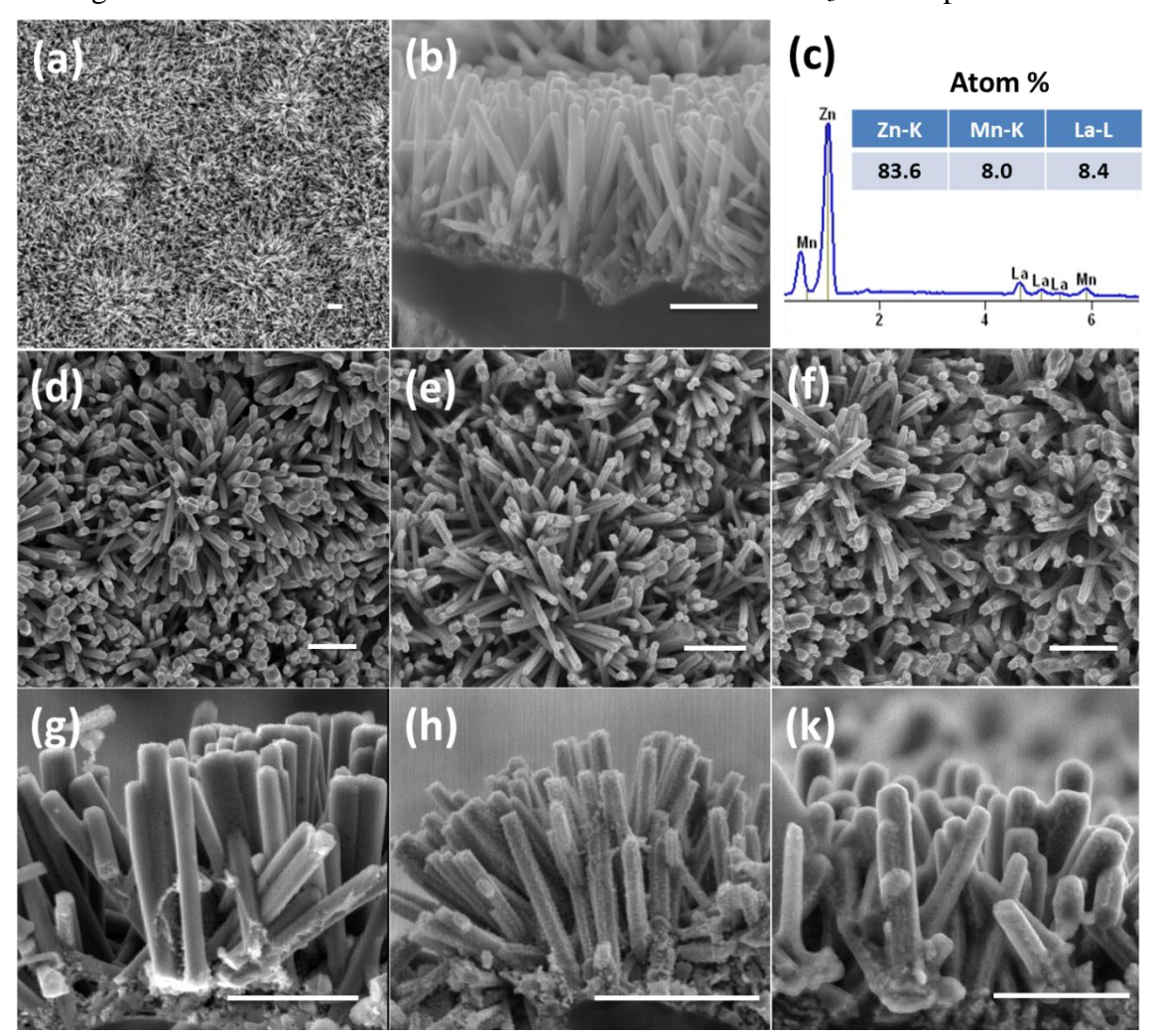


Figure 2. SEM images of (a) top view and (b) cross-section view of ZnO nanorod arrays rooted on monolithic cordierite substrate (d) top view and (g) cross-sectional view of ZnO/LMO core-shell nanorod arrays; (e) top view and (h) cross-sectional view of

ZnO/LCO core-shell nanorod arrays; (f) top view and (k) cross-sectional view of ZnO/LNO core-shell nanorod arrays; (c) EDXS spectrum corresponding to the sample in (d). Scale bars without labels are 1 μ m.

TEM characterization of ZnO/LCO and ZnO/LMO core-shell nanorods is presented in Figure 3. Perovskite LaCoO₃ particles can be clearly observed in bright (a) and dark (b) field images. The d-spacing values of {0 1 2} and {1 1 3} of LaCoO₃ lattice were labeled in Figure 3 (c). Figure 3 (d) shows the dark field image of a ZnO/LMO nanorod. The random distributed bright dots suggest LMO nanoparticles dispersed on ZnO nanorod. The thickness of perovskite coating can be increased by multiple colloidal wash coating cycles. And complete removal of residual solution before dried guarantees the uniformity of perovskite coating.

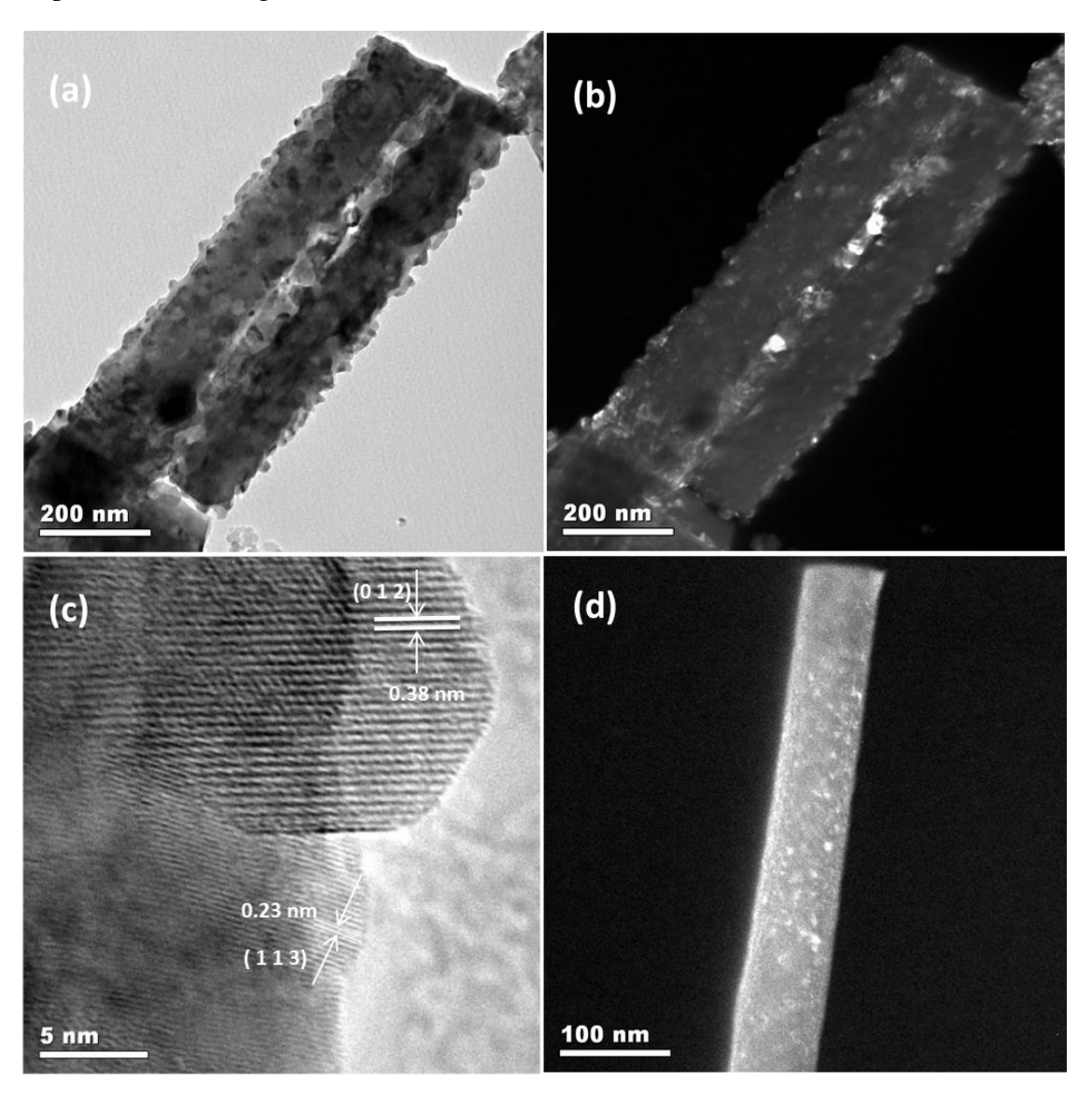


Figure 3. (a) Bright field and (b) dark field TEM images of ZnO/LCO core-shell nanorods; (c) HRTEM investigation of (a); (d) dark field TEM images of a ZnO/LMO core-shell nanorod.

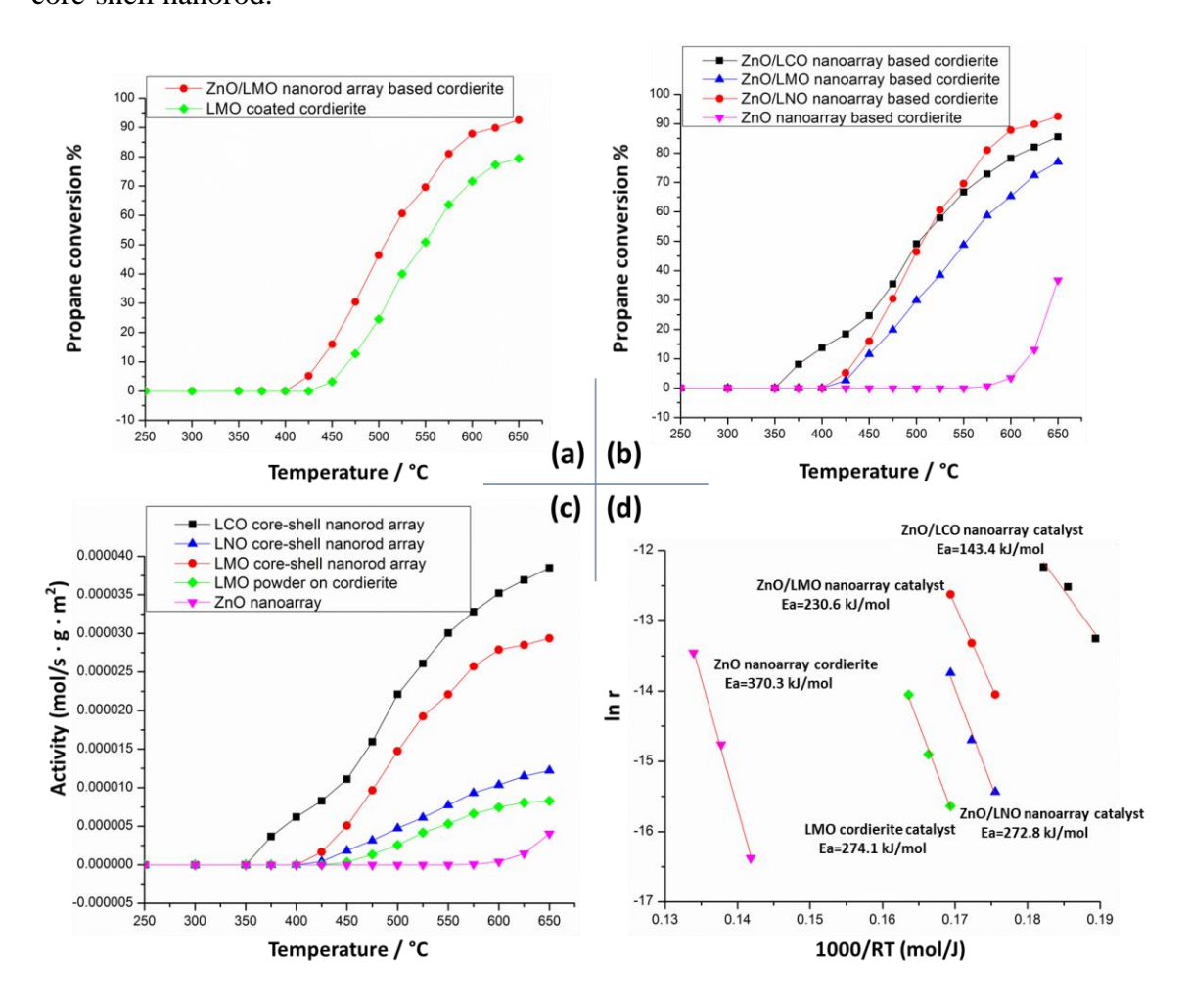


Figure 4. (a) Catalytic performance of powder-form LMO based and ZnO/LMO coreshell nanorod array based catalysts for propane oxidation; (b) catalytic performance of ZnO/LaBO₃ core-shell nanorod arrays based catalysts for propane oxidation; (c) activity of perovskite catalysts shown as a function of temperature; (d) corresponding Arrhenius plots for the reaction kinetics.

Figure 4 shows the propane oxidation light-off curves of core-shell nanorod arrays based cordierite samples and powder-form LMO coated cordierite sample as well as bare ZnO nanorod arrays based cordierite substrate. Compared to LMO coated monolithic sample, ZnO/LMO sample possesses a much lower light-off temperature (~25°C difference) and the activation energy is reduced from 274.1 kJ/mol (LMO) to 230.6 kJ/mol (ZnO/LMO), indicating an enchanced catalytic activity due to the ZnO/LMO core-shell nanorod structure. The improved performance may be attributed to good dispersion of LMO nanoparticles upon ZnO nano-array, facilitating the gas-solid interactions [8]. On the

other hand, the interfaces between LMO nanoparticles and ZnO nanorods support may also play an important role in catalytic performance improvement though direct evidence of interaction still needs further investigation [11]. In terms of lateral comparison of three types of ZnO/perovskte nano-array catalysts, ZnO/LCO sample shows the best catalytic performance at low temperature, with reaction initiated at 350°C of a significant propane conversion of over 13% where no conversion is detected for the other samples. However, ZnO/LCO and ZnO/LMO samples reach 50% conversion almost at same temperature (500°C) after which ZnO/LMO sample displays highest propane conversion until 650°C. Since the core-shell nanorod array based catalysts possess well-defined geometric characteristic as compared to LMO/cordierite catalyst, the reaction rate of propane oxidation was calculated in unit of mole per second per gram per square meter (mol/s.g.m²) of perovskite materials and presented in Figure 4 (c) as a function of temperature. The corresponding activation energies of three types of core-shell nanorod arrays based samples and LMO coated cordierite sample are presented in Figure 4 (d). The reaction rate (catalytic activity) is revealed in the order ZnO/LCO > ZnO/LMO> ZnO/LNO.

Figure 5 (a) shows the temperature programmed reduction (TPR) profiles of three monolithic samples under H₂ atmosphere. In general, complete reduction of Mn⁴⁺ is hardly achieved and Mn³⁺ acts as an intermediate status before reduced to Mn²⁺ [12,13]. For ZnO/LMO cordierite sample, a single major peak was observed between 350-400°C, which corresponds to the reduction of Mn⁴⁺ to Mn³⁺. The shoulder located at ~500°C can be ascribed to the excess oxygen and the reduction of ZnO nano-arrays. An initial consumption of H₂ was observed close to 800°C, which is attributed to the reduction of Mn³⁺ to Mn²⁺. For the profile of ZnO/LCO cordierite sample, two major peaks appeared, which coincide with previous reports [14,15] that Co³⁺ was first reduced to Co²⁺ (325-450°C), followed by reduction of Co²⁺ to Co⁰ at higher temperature (>600°C). Moreover, the complete reduction of LaNiO₃ is divided into three stages, where La₂NiO₄ is formed as an intermediate phase [16]. Only two peaks were observed in the TPR profile of ZnO/LNO sample. The first peak is attributed to the reduction of nickel oxide (300-400°C), with the second peak due to the reduction of Ni²⁺ to Ni⁰ (>550°C) [17]. In addition, it is worth noting that H2 intensity keeps dropping between the first and the second peaks in both ZnO/LCO and ZnO/LNO cordierite samples. This may result from the reduction of ZnO continuously consumed H₂ from 450 °C to 550°C [18]. Since the first peak for each sample displays very close reduction temperature, it is only concluded that the amount of surface lattice oxygen in ZnO/LCO is higher due to its higher H₂ consumption.

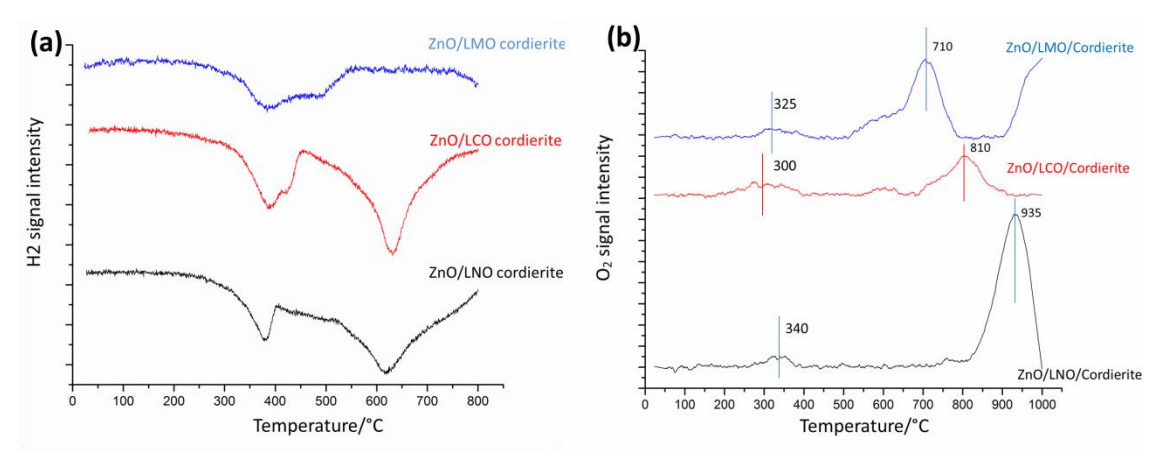


Figure 5. (a) H_2 Temperature-programmed-reduction and (b) Temperature-programmed-desorption of O_2 .

It has been widely reported that there are two types of oxygen species in perovskite materials, α and β oxygen. α oxygen is suggested to desorb at a low temperature range of 300-600°C, as determined by the amount of surface oxygen vacancy [15,19]. The peaks appeared at higher temperature (>600°C) correspond to the desorption of β oxygen, which is strongly associated with oxygen mobility in bulk [15,19]. To understand the oxygen evolution in the ZnO/perovskite core-shell nanorod arrays, temperature programmed desorption test was carried out. The O₂-TPD profiles are presented in Figure 5 (b). For α oxygen species, as compared to the other samples, ZnO/LCO cordierite possesses a broader peak at relatively low temperatures (300°C) while relatively weak peaks are located at 325°C for ZnO/LMO and 340°C for ZnO/LNO respectively, indicating the oxygen species absorbed on surface vacancies are more active and the amount is higher than the other two samples. In a higher temperature range, a strong peak appears at 810°C with a weak but detectable shoulder at 600°C. For ZnO/LMO cordierite, the temperature of β oxygen peak is much lower (710°C) than the other two samples, accompanied by a noticeable shoulder from 520°C to 650°C that can be related to excessive lattice oxygen in LaMnO_{3.5} [20]. No obvious shoulder was detected in ZnO/LNO cordierite, a strong peak is observed at 935°C. Therefore, the activity of surface lattice oxygen is in the order of ZnO/LCO > ZnO/LMO > ZnO/LNO, which corresponds to the catalytic activity observed in propane oxidation light-off curves in the low temperature range (<400°C)

It is well known that perovskite metal oxide provides oxygen in the a catalytic reaction while B cation is reduced, then the reduced metal is reoxidized by aquiring oxygen from surroundings [21]. Hence, the activity of surface lattice oxygen and the mobility of oxygen in bulk play important roles in a complete redox cycle [21,22]. The order of three catalysts' performances at low temperature matches the order of activities of surface lattice oxygen observed in TPD-O₂ characterization, as supported by Mars-Van Krevelen

mechanism [23]. As proposed, the surface lattice oxygen reacts with reactant molecule, leaving an oxygen vacancy on the surface of catalysts. The vacancy is filled by oxygen in gas phase or oxygen in bulk. For our samples, specifically, the mobility of oxygen in bulk is in the sequence of ZnO/LMO > ZnO/LCO > ZnO > LNO, which contradicts previous reports [14] that the oxygen mobility of LCO is more active than that of LMO in bulk. This can be demonstrated by the excessive lattice oxygen in LaMnO_{3.5}, which significantly enhanced catalytic activity of LaMnO_{3.5} at high temperature [24]. Furthermore, the excessive lattice oxygen may contribute to the replenishment of surface oxygen vacancies and enable better catalytic performance of ZnO/LMO than that of ZnO/LCO above 500°C. As a potential contribution, the influence of ZnO/LMO interface should be further investigated. According to our previous report [25], the thickness dependent ferromagnetic-superparamagnetic transition in (La, Sr)MnO₃ nanofilm on ZnO nanorod arrays was observed, which imposed another possible pathway to study catalytic activity improvement of ZnO/perovskite core-shell nanorod arrays based catalysts.

Conclusions

In summary, ZnO/LaBO3 (B = Co, Mn, Ni) core-shell nanorod arrays have been successfully grown on 3-D honeycomb cordierite substrate using a hydrothermal and colloidal deposition synthesis method. Compared to traditional wash-coated LMO monolith catalyst, an enhanced catalytic performance was observed for ZnO/LMO nanorod arrays based catalyst with 25°C lower light-off temperature than wash-coated perovskite catalyst of similar LMO loading (4.3mg). And the corresponding activation energy also shows a decrease from 274.1 kJ/mol for LMO/cordierite catalyst to 230.6 kJ/mol for ZnO/LMO nanorod arrays based catalyst. The good dispersion and size control in La-based perovskite nanoparticles and their interfaces to ZnO nanorod arrays support may be contribute to the enhancement of catalytic performance. The lateral comparison of three types of ZnO/LaBO3 nanorod arrays based catalysts reveals a catalytic activity sequence of LaCoO3 > LaMnO3 > La2NiO4 at the initial stage of catalytic reaction. This work may provide a new type of Pt-group metals (PGM) free catalysts with improved catalytic performance for hydrocarbon oxidation at low temperature.

Acknowledgement: The authors are grateful for the financial support from the US Department of Energy (Award # DE-EE0006854) and the National Science Foundation (Award # CBET-1344792). Z. R. would like to acknowledge the partial support from a General Electrics Graduate Fellowship for Innovation.

Reference:

[1] J. Lin, B. Qian, J. Liu, Y. Huang, A. Wang, L. Li, W. Zhang, L. F. Allard, X. Wang, T. Zhang, Angew. Chem. 123 (**2012**) 2974-2978.

- [2] X. Mou, B. Zhang, Y. Li, L. Yao, X. Wei, D. S. Su, W. Shen, Angew. Chm. Int. Ed. 51 (2012) 2989-2993.
- [3] M O'Connell, A.K Norman, C.F Hüttermann1, M.A Morris, Catal. Today. 47 (1999) 123.
- [4]. Nora A. Merino, BiBiana P. Barbero, J. Catal. 231 (2005) 232-244.
- [5] T. Asada, T. Kayama, H. Kusaba, Catal. Today. 139 (2008) 37-42.
- [6] Y. Lu, A. Eyssler, E. H. Otal, S. K. Matam, Catal. Today. 208 (2013) 42-47.
- [7] M. Alifanti, J. Kirchnerova, B. Delmon, D. Klvana, Appl. Catal. A, 262 (**2004**) 167-176.
- [8] Y. Guo, Z. Ren, W. Xiao, C. Liu. H. Sharma, H. Gao, A. Mhadeshwar, P.-X. Gao. Nano Energy. 2-5 (**2013**) 873-881.
- [9] Z. Ren, V. Botu, S. Wang, Y. Meng, W. Song, Y. Guo, R. Ramprasad, S. Suib, P.-X. Gao. Angew. Chem. Int. Ed. 53 (2014), 1-6.
- [10] W. Xiao, Y, Guo, Z. Ren, G. Wrobel, Z. Ren, T. Lu, P. X. Gao. Gryst. Growth Des. 13 (2013) 3657-3664.
- [11] D. Jian, P.-X. Gao, W. Cai, B.S. Allimi, S. Pamir Alpay, Y. Ding, Z. L. Wang, C. Brooks, J. Mater. Chem. 19 (**2009**) 970–975.
- [12] S. Irusta, M.P. Pina, M. Menéndez, J. Santamaria, J. Catal. 179 (1998) 400-412.
- [13] A. Kaddouri, S. Ifra, Catalysis Communication. 7 (2006) 109-113.
- [14] S. Royer, F. Bérubé, S. Kaliaguine, Appl. Catal. A 282 (2005) 273-284.
- [15] B. Levasseur, S. Kaliaguine, Appl. Catal. A 343 (**2008**) 29-38.
- [16] C. Batiot-Dupeyrat, G. Valderrama, A. Meneses, F. Martinez, J. Barrault, Appl. Catal. A 248 (2003) 143-151.
- [17] G. S. Gallego, F. Mondragón, J. M. Tatibouët, Catal. Today. 133-155 (**2008**) 200-209.
- [18] M. Liang, W. Kang, K. Xie, J. Natural Gas Chem. 18 (2009) 100-113.
- [19] K. Kaliaguine, A. Van Neste, V. Szabo, J. E. Gallot. M. Bassir, R. Muzychuk, Appl. Catal. A. 209 (**2001**) 345-358.

- [20] C. Zhang, Y. Guo, Y. Guo, G. Lu, A. Boreave, L. Retailleau, A. Baylet, A. Giroir-Fendler. Appl. Catal B. 148-149 (**2014**) 490-498.
- [21] M. Baldi, E. Finocchio, F. Milella, G. Busca, Appl. Catal B. 16 (1998) 43-51.
- [22] R. K. Grasselli, Topics in Catal. 21 (2002) 79-88.
- [23] B. C. Enger, R. Lødeng, Anders Holmen, Appl. Catal A. 346 (2008) 1-27.
- [24] L. Marchetti, L. Forni, Appl. Catal B. Environmental 15 (1998) 179-187.
- [25] H. Gao, M. Staruch, M Jain, P. Gao, P, Shimpi, Y. Guo, W. Cai, H. Lin, Applied Physics letters, 98 (2011) 123105.